Attempt to Evaluate the Building Factor of a Stator Core in Inverter-Fed Permanent Magnet Synchronous Motor

Nicolas Denis, *Member, IEEE*, Shunya Odawara, *Member, IEEE*, and Keisuke Fujisaki, *Senior Member, IEEE*

***Abstract*—This paper presents an attempt to evaluate the building factor of a stator core made of nonoriented silicon steel laminations. The stator core is used in a synchronous motor with buried permanent magnets driven by a voltage source three-phase inverter with classical pulse-width modulation (PWM) control. The building factor is the ratio between the iron loss density in the stator core and the specific iron loss density of the material. It then gives an evaluation of the impact of the core manufacture and the motor geometrical configuration on the stator iron losses. A first experiment is conducted to measure the iron losses of the inverter-fed motor in no-load condition. The material-specific iron losses are then evaluated by trying to apply similar magnetic flux density conditions in a wound laminated ring. The results show a decrease of the building factor with the PWM carrier frequency.**

***Index Terms*—Building factor, magnetic cores, magnetic flux density, magnetic losses, permanent magnet machines.**

I. Introduction

THREE-PHASE inverters are often used for torque, speed, and position control of electrical motors. Their basic function is to convert a constant dc voltage source into a three-phase quasi-sinusoidal voltage with controllable frequency and amplitude. The pulse-width modulation (PWM) technique results in high-frequency components in the inverter output voltage. In [1], the specific iron losses of magnetic materials are measured under two different winding excitations; purely sinusoidal voltage and PWM inverter output voltage. It is shown that the PWM inverter supplied voltage sensibly increases the iron losses compared to the sinusoidal voltage. The PWM is responsible for high-frequency components in the magnetic flux density and minor loops in the B–H curve that can explain such an increase [2]. Further investigations show that the specific material iron loss decreases with the PWM carrier frequency [2], [3], but also varies with the PWM modulation factor [3], the switching dead-time [4], and the semiconductor on-voltage [5].

In addition to the above investigations carried out with material sheet samples or wound ring cores, this phenomenon has also been studied with manufactured magnetic cores used in actual electrical motor applications. Similarly to the experimental protocols used in [1]–[5], an electrical motor can be driven with both purely sinusoidal voltage supply and PWM inverter output voltage supply. The measurements of the iron losses in both conditions and their comparison are assumed to give a rather accurate estimation of the impact of the PWM. In [6], the increment of iron losses in an induction motor (IM) due to the PWM is found to decrease quite sensibly with the carrier frequency but also depends on whether the IM works at no-load or drives a mechanical load. The complexity of the inverter-motor system makes the comprehension and prediction of the iron losses very difficult. However, for the sake of motor design, accurate predictions are often needed. As a consequence, Boglietti *et al.* have strived to improve analytical and numerical iron loss models of PWM inverter-fed IMs [7], [8]. The impact of the PWM on the iron losses of permanent magnet synchronous motors (PMSM) has also been investigated. In [9], experimental trials report an increase of the iron losses by 22% with a PWM carrier frequency of 10 kHz for a PMSM in no-load condition. Some authors also observed the decrease of the iron losses with the carrier frequency. In [10], for a 6.9 kW PMSM, the additional losses due to the carrier frequency decreases by about five times when the carrier frequency ratio (ratio of carrier frequency over fundamental frequency) increases from 5 to 80. An analysis of the total losses of an inverter plus PMSM drive system is proposed in [11]. Observing that increasing the carrier frequency concurrently decreases the iron losses of the motor and increases the inverter switching losses, Sato and Itoh proposed a way to select the optimal carrier frequency for maximum efficiency operation.

The iron loss phenomenon in an inverter-fed PMSM is more complex than the specific material iron loss measured under similar inverter excitation. Time harmonics, caused by the magnet shape and stator slots, appear in the magnetic flux density, which would increase the iron losses [12]. Consequently, authors worked on optimizing stator slot, magnet, and rotor surface shapes to decrease the iron losses [13]–[15]. Other factors of iron loss increase in an electrical motor application are the

Manuscript received December 23, 2015; revised April 13, 2016; accepted April 28, 2016. Date of publication June 1, 2016; date of current version February 9, 2017. This work was supported in part by the Ministry of Education, Culture, Sports, Science, and Technology, Japan, program for private universities.

The authors are with Toyota Technological Institute, Nagoya 468-8511, Japan (e-mail: nicolas.denis@toyota-ti.ac.jp; sodawara@toyota-ti.ac.jp; fujisaki@toyota-ti.ac.jp).

Color versions of one or more of the figures in this paper are available online at http://ieeexplore.ieee.org.

Digital Object Identifier 10.1109/TIE.2016.2573267

0278-0046 © 2016 IEEE. Personal use is permitted, but republication/redistribution requires IEEE permission.
See http://www.ieee.org/publications_standards/publications/rights/index.html for more information.

TABLE I
MATERIAL CHARACTERISTICS

Reference	35H300
Composition	Fe–Si
Thickness (μm)	350
Saturation magnetic flux density (T)	2.12
Resistivity ($\mu\Omega.\mathrm{m}$)	0.5
Iron loss density at 50 Hz and 1 T (W/m^3)	11.4×10^3
Iron loss density at 50 Hz and 1.5 T (W/m^3)	37.2×10^3

rotating magnetic flux and magnetic anisotropy [16]–[18], but also the stress the material is subjected to during the manufacture process [19].

The building factor (BF) of any magnetic core is defined as the ratio between the iron loss density of the core (when used in a given application) and the specific iron loss density of the material. Its evaluation is important to understand and measure the iron losses caused by factors not related to the material itself. These factors can be the manufacture process, the core geometrical configuration, or even some effects of the operating conditions of a given application. BFs are traditionally evaluated in transformers [20] and reactors [21]. It is more difficult to measure the BF of a motor stator core because of the complexity in geometry and magnetic flux density distribution, but also due to the difficulties in measurements. In [22], a method is proposed to measure the BF caused by the punching technique on soft magnetic materials, by means of experimental trials on wound cores. The results are then used to predict the iron losses in an IM stator core.

In this paper, a method is proposed to evaluate the BF of the stator core of a PMSM with interior magnets (IPMSM) by direct measurements on the rotating motor. The iron losses and magnetic flux density are first measured on the inverter-fed IPMSM at no-load. Then two-dimensional (2-D) finite-element analysis (FEA) is performed in order to make assumptions and approximations on the magnetic flux density and iron loss distribution. Finally, tests are carried out to replicate similar conditions in wound ring cores, measure their iron losses, and then calculate the BF of the IPMSM stator core.

II. MATERIAL CHARACTERISTICS AND MOTOR GEOMETRY

A. Material Characteristics

The stator and rotor cores of the proposed IPMSM are made of nonoriented electrical steel sheets cut using a wire cut technique to reduce the deterioration of the magnetic properties by mechanical stress. The important characteristics of the material are summed up in Table I. The *B–H* characteristic and the specific iron loss characteristic have been measured by single sheet test and are given in Figs. 1 and 2, respectively.

B. Motor Geometry

The motor proposed in this paper is a synchronous motor with buried permanent magnets. The cross section geometry is illustrated in Fig. 3. Sintered NdFeB magnets with a residual magnetization of 1.28 T and a resistivity of 1.6 $\mu\Omega$·m are

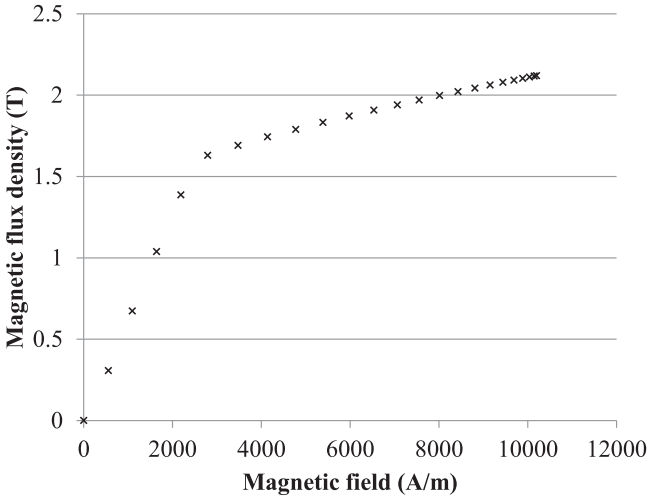

Fig. 1. *B–H* characteristic of the 35H300 material.

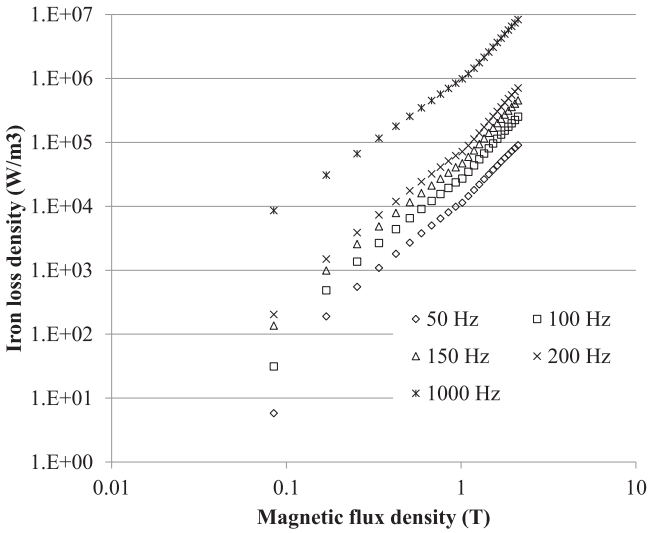

Fig. 2. Specific iron loss density of the 35H300 (logarithmic scale).

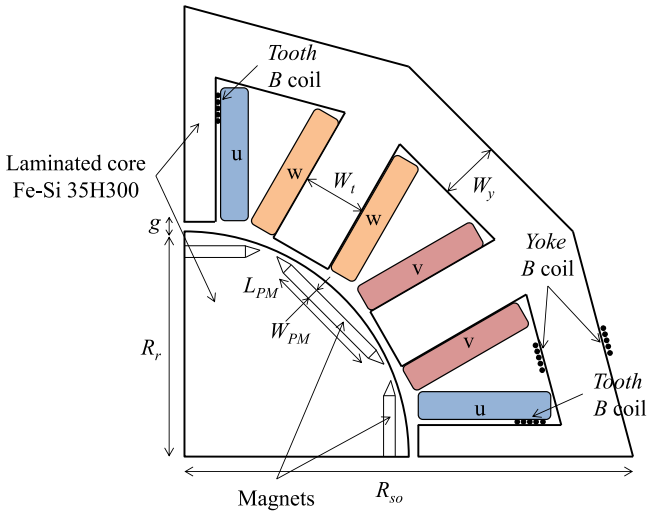

Fig. 3. Quarter cross section of the proposed IPMSM.

TABLE II
IPMSM GEOMETRICAL CHARACTERISTICS

Poles/Slot number	8/12
Radius of stator core R_{so}	64 mm
Radius of rotor core R_r	37 mm
Air gap g	1.25 mm
Yoke width W_y	9.2 mm
Tooth width W_t	10 mm
Magnet length L_{PM}	20 mm
Magnet thickness W_{PM}	2 mm
Core length L_c	47 mm
Number of winding turns	37

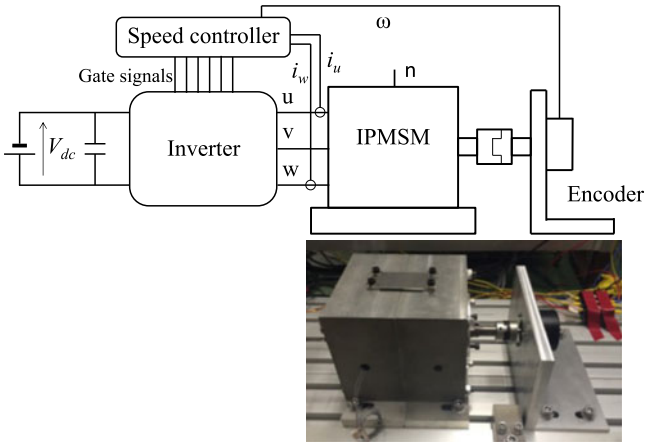

Fig. 4. No-load test experimental test bench.

used. The stator is wound using the concentrated method. The geometry characteristics are listed in Table II.

III. NO-LOAD EXPERIMENTAL TRIALS

In this paper, it is proposed to measure the iron losses of the IPMSM at no-load condition. Here, the total iron losses of the IPMSM are the hysteresis and eddy-current losses in the magnets, rotor, and stator. The experimental test bench is illustrated in Fig. 4. The IPMSM is driven by a three-phase voltage source inverter with IGBTs and a constant dc voltage source provides the power to the inverter. A standard vector control with PWM is implemented and the d-axis current reference is set to zero. No-load is connected to the output shaft but an encoder is still needed for the speed feedback.

The IPMSM input active electrical power $P_{3\Phi}$ is measured by a power analyzer using the equation

$$P_{3\Phi} = \frac{1}{n}\sum_{k=1}^{n-1}\left(i_u(k)v_{un}(k) + i_v(k)v_{vn}(k) + i_w(k)v_{wn}(k)\right) \tag{1}$$

where $i_{u,v,w}$ are, respectively, the u-, v-, and w-phase currents, $v_{\mathrm{un,vn,wn}}$ are, respectively, the u-, v-, and w-phase-to-neutral voltages, and n is the sample number in an integral number of electrical periods. The measurement sampling frequency is 2.2 MHz. In order to calculate the copper losses, the rms current has also been calculated from the sampled current waveform using the equation

$$I_{\mathrm{xrms}} = \sqrt{\frac{1}{n}\sum_{k=0}^{n-1} i_x^2(k)} \tag{2}$$

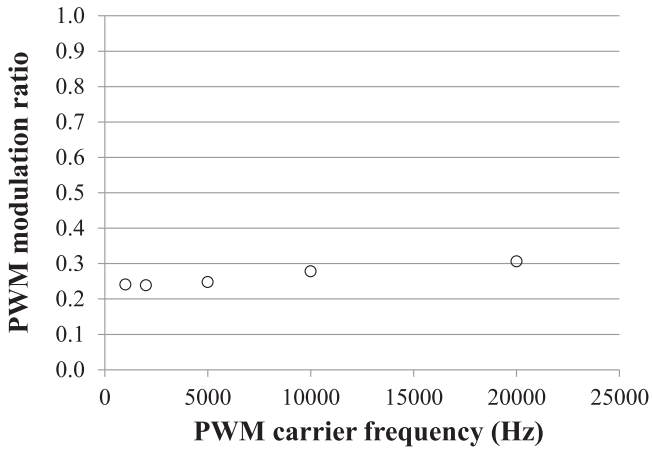

Fig. 5. PWM modulation ratio variation with the carrier frequency.

where x can be u, v or w depending on the considered phase.

The iron losses under no-load can then be calculated using

$$P_{i\_\mathrm{mot}} = P_{3\Phi} - R_s\left(I_{\mathrm{urms}}^2 + I_{\mathrm{vrms}}^2 + I_{\mathrm{wrms}}^2\right) - P_{\mathrm{mech}} - P_{\mathrm{enc}} \tag{3}$$

where R_s is the phase-to-neutral winding resistance measured under the dc condition, and P_{mech} and P_{enc} are the mechanical losses of the IPMSM and the encoder, respectively. The mechanical losses are previously measured by substituting the rotor with magnets by a rotor without magnets, but with the same shape and identical bearings. The IPMSM without magnets is then rotated by an external brushless DC motor and a torque meter is used to measure the torque needed to rotate the shaft at a given speed. The obtained torque represents the mechanical losses.

The tests are performed at a rotational speed of 750 r/min (electrical frequency f_e of 50 Hz). The dc-bus voltage V_{dc} is set to 180 V. The PWM carrier signal is a standard triangular shaped waveform varying between –1 and 1 with a constant frequency. The switching dead-time is set to 3500 ns. Five experimental tests with different carrier frequencies f_c, ranging from 1 to 20 kHz, have been performed. Fig. 5 illustrates the variation of the PWM modulation ratio over the five tests. Since the dead-time is constant at each tested carrier frequency, the ratio between the IGBT on-time and the dead-time decreases with the carrier frequency. Given that V_{dc} is constant, the fundamental phase voltage at the output of the inverter would then decrease with the carrier frequency if the modulation ratio stays constant. However, the same fundamental phase voltage is required at each test since the speed remains the same. This automatically means that the modulation ratio has to increase with the carrier frequency in order to adjust the inverter output fundamental voltage [23].

B coils are wound on the stator teeth and yokes, as illustrated in Fig. 3, with a pattern of one coil per pole pairs (four on the yokes and four on the teeth). The B coils provide a voltage value V_B used to calculate the average magnetic flux density $B_{\mathrm{avg\_}s}$ at time t through the tooth or yoke radial section. The

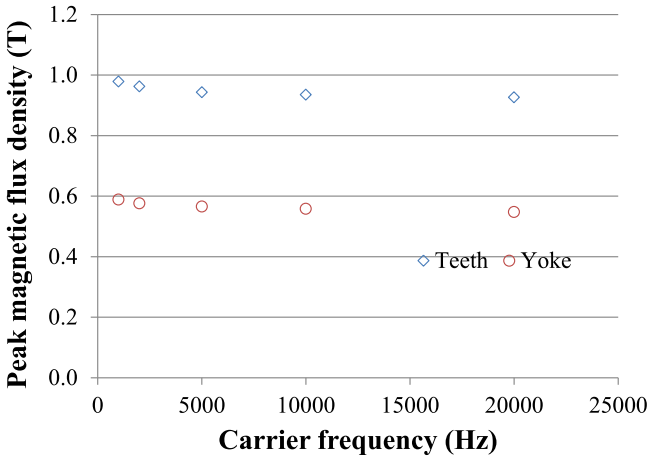

Fig. 6. Peak magnetic flux density in the teeth and yokes (average among the four coils).

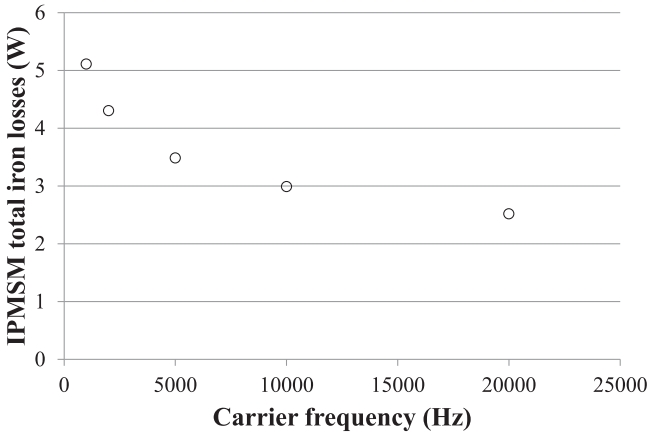

Fig. 7. IPMSM total iron losses at no-load, 750 r/min.

corresponding equation is

$$B_{\text{avg\_}s}(t) = \frac{1}{N_B S_c} \int_0^t V_B(u)\, du \tag{4}$$

where N_B is the number of turns of the B coil and S_c is the tooth or yoke radial section area, depending on which coil is considered. The calculation of $B_{\text{avg\_}s}$ through the measurement of V_B during operation shows a disparity in the peak values of the magnetic flux waveforms among the four teeth or yoke parts. It can be caused by either a slight axial misalignment of the rotor or a small nonuniformity in the winding of the B coil. Consequently, it is proposed to assign a single value to the peak magnetic flux in the teeth or yoke, which is the average peak value among the four coils. Fig. 6 illustrates the variation of the above defined peak magnetic flux density with the carrier frequency. It can be observed that the magnetic flux level is kept below the saturation level (see Fig. 1). This excludes any adverse effect that the saturation could have on the later calculated BF. Finally, Fig. 7 shows the evolution of the IPMSM total iron losses with the carrier frequency. Fig. 8 illustrates the magnetic flux density measured by one of the tooth coil and compares the

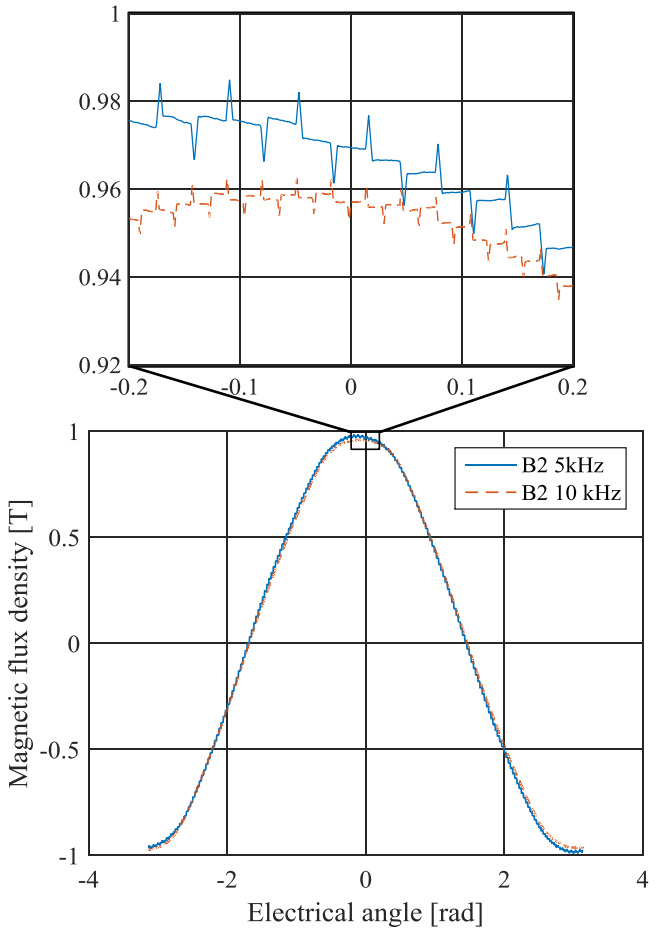

Fig. 8. Comparison of the magnetic flux density in the teeth part at $f_c = 5$ kHz and $f_c = 10$ kHz.

cases where the carrier frequency is 5 and 10 kHz. On the scale of the carrier signal period, the magnetic flux density waveform has a periodic uneven shape whose frequency increases with the carrier frequency. Its peak to peak value, however, decreases. This results in a decrease of iron losses.

IV. Finite-Element Analysis

The previous experimental trials give the total motor iron losses but not the loss repartition between the stator, rotor, and magnets. As will be explained in a later section, an approximation of the repartition is needed for the BF calculation of the stator core. Such approximation can be done using FEA. The working conditions described in the previous section are simulated by 2-D finite element method using the JMAG software. To this end, the phase current waveforms measured during the experimental trials are used as an input of the numerical analysis.

A. Estimation of Iron Loss in the Stator and Rotor

In the stator and rotor, the equation of the vector potential $\boldsymbol{A}$ is solved without considering the eddy currents

$$\frac{\partial}{\partial x}\left(\nu_y \frac{\partial A_z}{\partial x}\right) + \frac{\partial}{\partial y}\left(\nu_x \frac{\partial A_z}{\partial y}\right) = -J_0 \tag{5}$$

where A_z is the axial component of the vector potential, ν_x and ν_y are the magnetic reluctivity on the x- and y-axis, respectively, and J_0 is the current density in the coil parts. In our case, ν_x and ν_y are equal since the electrical steel is considered magnetically isotropic.

The analysis consists in a time-stepped simulation, spanning a rotor rotation angle of 90° (one electrical period). The radial and tangential magnetic flux densities B_r and B_θ are calculated solving (5) in each mesh of the 2-D model. A fast Fourier transform is then performed to find the time harmonic components of B_r and B_θ. The iron loss density W_e in each mesh of the model is calculating using the Steinmetz equation

$$W_e = \sum_{i=1}^{N_h} \left(k_{h,i} f_i \left(B_{r,i}^2 + B_{\theta,i}^2 \right) + k_{e,i} f_i^2 \left(B_{r,i}^2 + B_{\theta,i}^2 \right) \right) \quad (6)$$

where i is the harmonic rank, N_h is the rank of the highest harmonic, f_i is the frequency of the ith harmonic, $B_{r,i}$ and $B_{\theta,i}$ are the amplitudes of the ith harmonic of the radial and tangential components of the magnetic flux density, respectively, and $k_{h,i}, k_{e,i}$ are the Steinmetz constants of the hysteresis and eddy current losses, respectively, which are estimated from the data of Fig. 2 and depend on the frequency.

The magnets shape is responsible for a low-frequency harmonic distortion of the magnetic flux in the stator parts. Similarly, the PWM carrier frequency is responsible for a high-frequency harmonic distortion. These two phenomena especially increase the eddy current losses in the stator [24]. In (6), this is taken into account by the magnetic flux harmonics in the second term of the sum.

The low-frequency harmonics of the magnetic flux do not really impact the hysteresis losses but the PWM carrier frequency is responsible for minor loops in the *B–H* curve that increase them [25]. In this case, one evaluation method consists of summing the hysteresis losses related to the major loop and the hysteresis losses of each minor loop using the Preisach model [25]. Some more calculation-friendly equations also exist, considering for example the local amplitude of the flux density that causes minor loops and the number of minor hysteresis loops [26]. Consequently in (6), considering all the magnetic flux harmonics in the estimation of the hysteresis losses probably leads to inaccuracies.

Moreover, the magnetic flux in the stator is usually alternating in time but also in space, making it rotating with an elliptical locus. This phenomenon is likely to increase the iron losses compared to the case of a unidirectional alternating flux and it can be assessed in analysis equations using the ellipse characteristics [16]. In (6), only the peak value of the norm of the flux density vector is considered but the rotational characteristic is not.

In the light of the above clarifications, (6) can only be seen as an approximation. However, this equation has also been adopted in [12] with good agreement between experiment and calculation (maximum calculated error of about 15%). Considering the aim of this paper, it is thought that the accuracy provided by (6) is enough.

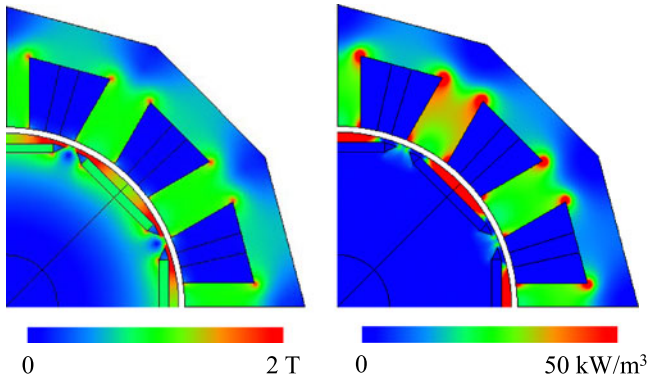

Fig. 9. Magnetic flux density (left) and iron loss density (right) distributions at no-load, $f_c = 1$ kHz, and 750 rpm.

B. Estimation of the Iron Losses in the Magnets

In the magnets, the equation of the vector potential is solved considering the eddy currents

$$\frac{\partial}{\partial x}\left(\nu_0 \frac{\partial A_z}{\partial x}\right) + \frac{\partial}{\partial y}\left(\nu_0 \frac{\partial A_z}{\partial y}\right) = -J_0 + \sigma_m \frac{\partial A_z}{\partial t} \quad (7)$$

where σ_m is the electrical conductivity of the magnet, ν_0 is the reluctivity of the vacuum, and the second term of the left side of the equation represent the eddy current density that will be noted J_s.

The hysteresis losses in the magnets are considered null. The eddy current loss density in each mesh can be estimated from the eddy current density using

$$W_m = \frac{1}{T} \sum_{i=1}^{N_i} \frac{J_s^2(i)}{\sigma_m} dt \quad (8)$$

where N_i is the number of time samples, T is the period duration, and dt is the time sampling duration.

C. Results of the FEA

Due to the high frequency of the PWM carrier signal, it is preferable to have a high sampling frequency on the current data input in the numerical analysis. This means small time-step and then long calculation. In order to reduce the calculation time, only the case $f_c = 1$ kHz has been simulated. In this case, the sampling frequency is set to 0.1 MHz. Fig. 9 illustrates the distribution of the maximum magnetic flux density occurring in the stator, rotor, and magnet parts during the simulated rotation. The figure also illustrates the distribution of the iron loss density in the rotor and stator parts. In accordance with the experimental tests, the magnetic flux density in the teeth parts is sensibly higher than in the yoke parts. Table III shows the calculated iron losses in the stator, rotor, and magnets. The stator iron losses account for 64% of the total iron losses and the calculated total iron losses are about 2 W higher than the measurement at $f_c = 1$ kHz (see Fig. 7).

TABLE III
IRON LOSS FEA CALCULATION RESULTS AT 750 R/MIN

	Iron losses (W)
Stator	4.531
Rotor	1.019
Magnet	1.522
Total	7.072

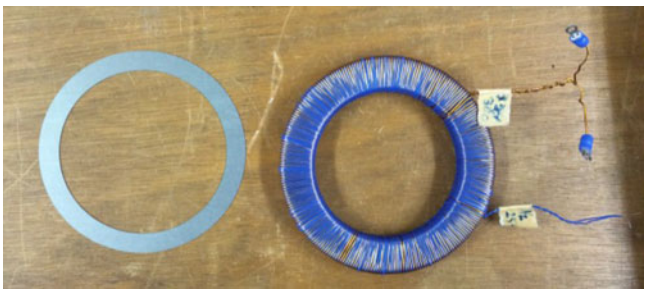

Fig. 10. Ring lamination (left) and wound ring core (right).

V. MEASUREMENT OF MATERIAL IRON LOSS DENSITY BY RING TESTS

The calculation of a BF usually requires the measurements of both the manufactured core iron losses and the material specific iron losses. It is proposed here to evaluate the specific iron losses by measurement on a wound ring core. The ring core, illustrated in Fig. 10, is composed of 20 ring laminations of a material identical to that used in the IPMSM stator core (35H300). The ring laminations were cut using wire cutting technique (same technique as used for the stator core laminations) and no heat treatment was performed after cutting. The ring has the same outer diameter as the stator.

Two kinds of ring tests are performed. Since, in no-load condition, the IPMSM stator windings are excited by a PWM voltage, the first ring test is performed under single-phase PWM excitation. However, it is also important to evaluate the specific material iron losses following excitation conditions that meet the international [27] and national standards [28]. As a consequence, a second test under sinusoidal excitation is performed.

A. Ring Under Inverter Excitation

The first ring test consists of exciting the ring core winding with a two-phase-leg inverter as illustrated in Fig. 11. The gate signals of the IGBTs are produced by PWM and the modulation signal of the first phase-leg (u_1) is the opposite of the second phase-leg (u_2) modulation signal. In order to reproduce similar conditions to those of the no-load test of Section III, the PWM modulation ratio is set identical to Fig. 5, the modulation signal frequency is set to 50 Hz, and the switching dead-time is set to 3500 ns. Tests are done at carrier frequencies of 1, 2, 5, 10, and 20 kHz, and the peak magnetic flux density in the ring core is adjusted by tuning the dc-bus voltage. During no-load tests, magnetic flux densities in teeth and yokes were measured, giving the two series of data for the peak magnetic flux density in the stator core, as illustrated in Fig. 6. As a consequence, it

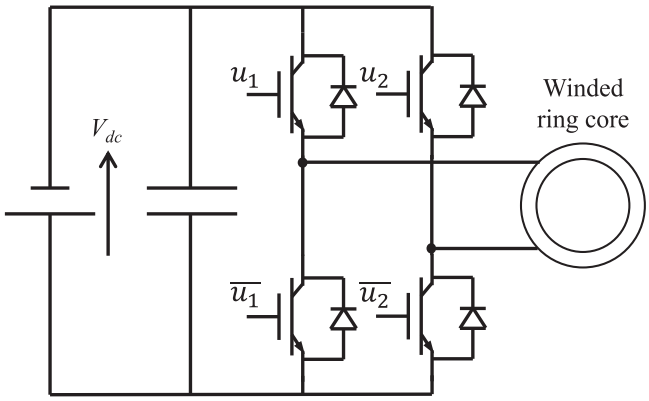

Fig. 11. Wound ring core under two phase-leg inverter excitation.

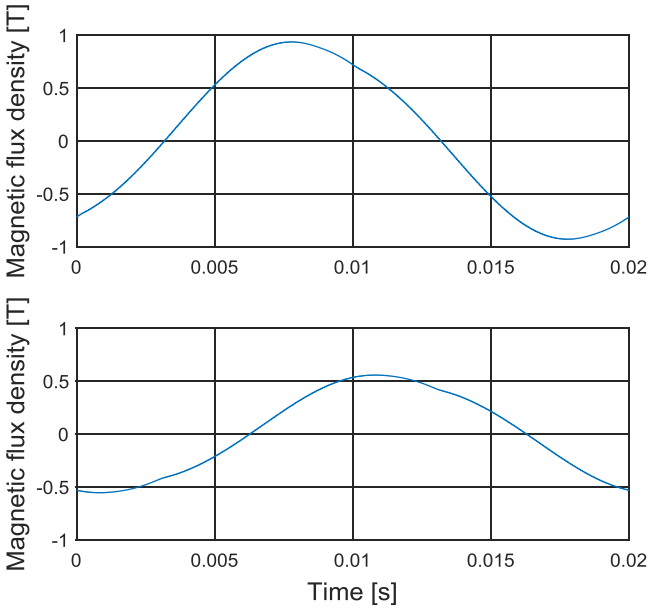

Fig. 12. Magnetic flux density in the ring core at $f_{\neg e} = 10$ kHz and $f_e = 50\ Hz$, teeth level (above) and yoke level (under).

is proposed here to carry out two series of ring tests; the first setting the ring core peak magnetic flux density close to the yoke one and the second close to the teeth one.

The ring magnetic flux density can be measured using the *B* coil (see blue wire in Fig. 10) wound with the main copper winding. The *B* coil voltage and the winding current are measured so that the average magnetic flux density through the ring core radial section $B_{\mathrm{avg\_r}}(t)$ and the magnetic field $H(t)$ can be estimated, respectively [2]. Then, the ring core iron loss density $W_{\mathrm{mat}}(\mathrm{W/kg})$ can be calculated using

$$W_{\mathrm{mat}} = \frac{\int H \cdot dB}{m_{\mathrm{ring}}} \tag{9}$$

where m_{ring} is the ring core mass. It should be noted that this formulation includes eddy current and hysteresis losses calculation and gives results very close to the calculation of power balance [29].

Fig. 12 illustrates the magnetic flux density measured in the ring core at a carrier frequency of 10 kHz for the two tested

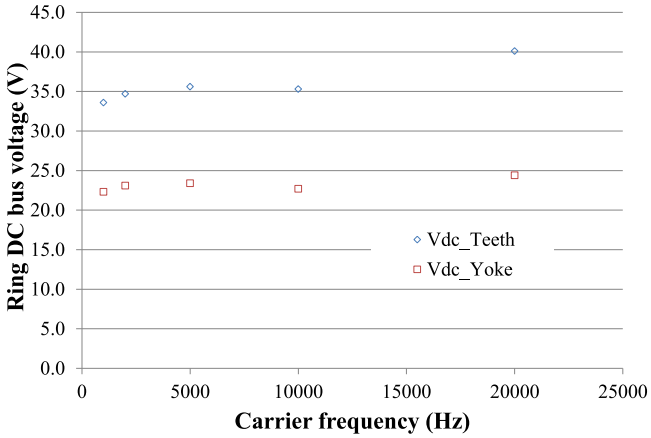

Fig. 13. DC-bus voltage needed to obtain the required peak magnetic flux density in the ring core. Teeth level (blue) and yoke level (red).

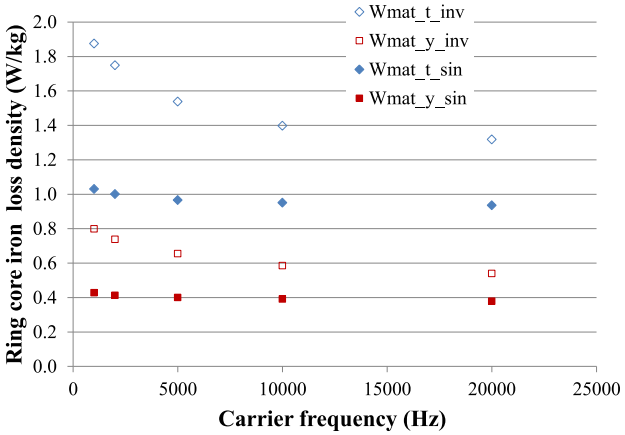

Fig. 14. Iron loss density measurement of ring core, teeth and yoke magnetic flux levels, sine-fed and inverter-fed.

peak levels (yoke and teeth levels as explained above). The dc-bus voltage needed to obtain the required peak magnetic flux density in the ring is illustrated in Fig. 13. As it can be seen, it is sensibly lower than the dc-bus voltage needed for the IPMSM no-load test. The ring core iron loss densities obtained with a magnetic flux density level close to the teeth value and yoke value are called $W_{\mathrm{mat\_t\_inv}}$ and $W_{\mathrm{mat\_y\_inv}}$, respectively.

B. Ring Under Sinusoidal Excitation

The second test consists of exciting the ring core winding with a purely sinusoidal voltage using a signal generator and a linear amplifier. In this manner, the ring core iron losses are not affected by the PWM carrier frequency, contrarily to the first test. The frequency of the sinusoidal voltage is set to 50 Hz and its peak value is adjusted to obtain the required magnetic flux density of Fig. 6. The iron loss density is measured in the same way as the first ring test, using (9), and is called $W_{\mathrm{mat\_t\_sin}}$ or $W_{\mathrm{mat\_y\_sin}}$, depending on whether the teeth level magnetic flux or the yoke level is applied in the ring core, respectively.

Ten measurements have been performed for both the inverted-fed ring test and the sine-fed ring test. The results are illustrated in Fig. 14. It should be noted that $W_{\mathrm{mat\_t\_sin}}$ and $W_{\mathrm{mat\_y\_sin}}$ do not depend on the carrier frequency, as it might be understood from Fig. 14, since no PWM is used when the ring winding is under sinusoidal excitation. However, they depend on the peak magnetic flux density, which, itself, varies with the carrier frequency, as illustrated in Fig. 6. The results have been presented this way in order to make the comparison easier.

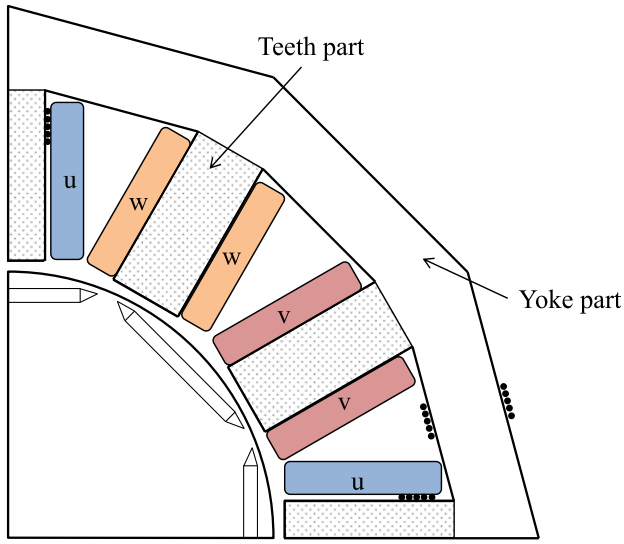

Fig. 15. Delimitation of yoke and teeth parts.

VI. BF Calculation

The aim of this paper is to try to evaluate the BF of the IPMSM stator core. To do so, it is proposed to compare the iron loss density (W/kg) of the ring core to the iron loss density of the stator core. While the iron loss density of the ring core has been measured in the previous section, the iron loss density of the stator core is not as straightforward because, contrary to the ring core, the magnetic flux density in the core has a lot of nonuniformity, as one can see in Fig. 9. As demonstrated in Sections III and IV, the magnetic flux density in the yoke and teeth parts are sensibly different from each other. As a consequence, it is proposed to delimit the yoke and teeth parts considering the uniformity of the magnetic flux density. The FEA of Fig. 9 is used for this purpose. By identifying the areas where the magnetic flux density is relatively uniform, the delimitation is done as in Fig. 15.

Knowing that two regions are distinctly considered in the stator, it is proposed to use the ring core iron loss density measurements at teeth and yoke magnetic flux levels (previous section), for the BF calculation. Moreover, since the measurements in Section III give the iron losses of all parts of the IPMSM (magnets, rotor, and stator), it is proposed to use a ratio to identify the iron losses in the stator only. This ratio is estimated from the FEA (64%). Consequently, the BF can be formulated as the ratio between the stator iron loss density and the ring core iron loss density as

$$BF = \frac{\frac{0.64 * P_{i\_\mathrm{mot}}}{m_y + m_t}}{\frac{W_{\mathrm{mat\_t}} * m_t + W_{\mathrm{mat\_y}} * m_y}{m_y + m_t}} \tag{10}$$

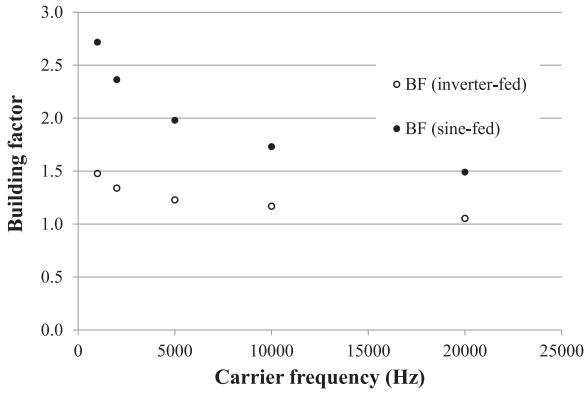

Fig. 16. BF calculation results considering both inverter-fed and sine-fed ring tests.

where m_y and m_t are the mass of the yoke part and the teeth parts, respectively, $W_{\mathrm{mat\_t}}$ can be either $W_{\mathrm{mat\_t\_inv}}$ or $W_{\mathrm{mat\_t\_sin}}$, and $W_{\mathrm{mat\_y}}$ can be either $W_{\mathrm{mat\_y\_inv}}$ or $W_{\mathrm{mat\_y\_sin}}$ depending on whether the inverter-fed ring test or the sine-fed ring test is considered for the calculation. The stator iron losses, given by the numerator in (10), are calculated as a portion of the IPMSM total iron losses. The ring iron loss density, given by the denominator in (10), is a weighted average between $W_{\mathrm{mat\_t}}$ and $W_{\mathrm{mat\_y}}$, with m_t ant m_y as weight coefficients.

Fig. 16 gives the BF calculation results for every tested carrier frequencies. As expected by the results of Fig. 14, the BF differs with the type of ring test that is considered for the ring iron loss density. When the inverter-fed ring test is considered [$W_{\mathrm{mat\_t\_inv}}$ and $W_{\mathrm{mat\_y\_inv}}$ in (10)], the BF values versus the carrier frequency are drawn in white dots. When the sine-fed ring test is considered [$W_{\mathrm{mat\_t\_sin}}$ and $W_{\mathrm{mat\_y\_sin}}$ in (10)], the BF values versus the carrier frequency are drawn in black dots. Since $W_{\mathrm{mat\_t\_inv}}$ and $W_{\mathrm{mat\_y\_inv}}$ are larger than $W_{\mathrm{mat\_t\_sin}}$ and $W_{\mathrm{mat\_y\_sin}}$, the BF calculated based on $W_{\mathrm{mat\_t\_inv}}$ and $W_{n\mathrm{mat\_y\_inv}}$ (inverter-fed) is larger.

In order to understand the meaning of the calculated BF here, it is important to define the relationships between the iron loss density given by the manufacturer data, the iron losses in a ring and the iron losses in an IPMSM stator.

The manufacturer data are considered to give an evaluation of the intrinsic material iron loss density for a range of frequency and induction values. It means that the iron losses are considered to depend exclusively on the material and no adverse effect contributes to the losses.

The wound ring is composed of cut rings of electrical steel. The cutting usually deteriorates the material in the vicinity of the cut line and this deterioration increases the iron losses. Then the ring test under sinusoidal excitation gives an iron loss density caused mainly by the material itself and the cutting. By comparing with the manufacturer data, it is then possible to evaluate the iron loss density increase due to the cutting for a given ring geometry.

Whenever the ring is excited by a PWM voltage waveform, the high-frequency harmonic of the PWM carrier increases the iron loss density compared to the case when the ring is excited by a sinusoidal voltage. As a consequence, the impact of the PWM carrier frequency on the iron loss density of the material can be evaluated by a simple comparison.

In the inverter-fed IPMSM under no-load, the iron losses in the stator core are caused by the same phenomena as in the ring core under inverter excitation, plus extra phenomena. These extra phenomena are 1) the fact that the magnetic flux is not only alternating but also rotating [16], [17]; 2) the effect of the magnet shape that distorts the magnetic flux density in the stator [12]; and 3) the geometry of the rotor + magnets + stator assembly that creates a particular path for the magnetic flux from silicon steel to magnets to air. More precisely, for the latter, the air gap is responsible for fringing flux that occurs at the end of the core and locally increase the eddy currents [30]. Interestingly, it has been proven for reactors with air gap that this effect decreases with the frequency [21], which could explain the decreasing trend observed on the BF.

To discuss the credence of the results in Fig. 16, it should be noted that two main approximations may lead to inaccuracies. At first, as previously explained, there are approximations in (6) for the numerical calculation. Considering the small difference between the experiments and the numerical calculation reported in [12], it is thought that these approximations have only a small negative effect on the accuracy of the BF. Second, because of the restricted possibilities of magnetic flux measurement on the stator core, the nonuniform distribution of the magnetic flux density has been brought down to two areas of the cross section (teeth and yoke areas), in which the magnetic flux is considered almost uniform. Considering the magnetic flux distribution of Fig. 9 calculated by FEA, in which a clear difference can be seen between the two areas, the proposed separation does not seem to be inappropriate. Consequently, it is thought that the accuracy of the BF does not suffer too much from this approximation.

VII. Conclusion

This paper presented an attempt to evaluate the BF of the stator core of an IPMSM under inverter-fed excitation in order to evaluate the impact of the manufacture and the geometrical configuration on the iron losses. Measurement difficulties lead to necessary approximations in the calculation but it can be concluded that, interestingly, the BF decreases with the PWM carrier frequency. Future work should concentrate on determining the main factor that causes the observed behavior of the BF.

References

[1] A. Boglietti, P. Ferraris, M. Lazzari, and F. Profumo, "Iron losses in magnetic materials with six-step and PWM inverter supply [induction motors]," *IEEE Trans. Magn.*, vol. 27, no. 6, pp. 5334–5336, Nov. 1991, doi 10.1109/20.278830.

[2] K. Fujisaki, R. Yamada, and T. Kusakabe, "Difference in iron loss and magnetic characteristics for magnetic excitation by PWM inverter and linear amplifier," *IEEJ Trans. Ind. Appl.*, vol. 133, no. 1, pp. 69–76, 2013, doi 10.1541/ieejias.133.69.

[3] M. Kawabe, T. Nomiyama, A. Shiozaki, H. Kaihara, N. Takahashi, and M. Nakano, "Behavior of minor loop and iron loss under constant voltage type PWM inverter excitation," *IEEE Trans. Magn.*, vol. 48, no. 11, pp. 3458–3461, Nov. 2012, doi 10.1109/TMAG.2012.2198199.

[4] S. M. Dehghan and K. Fujisaki, "Impact of dead-time on iron losses in inverter-fed magnetic materials," in *Proc. IEEE Energy Convers. Congr. Expo.*, Denver, CO, USA, Sep. 2013, pp. 3166–3171, doi 10.1109/ECCE.2013.6647115.
[5] K. Fujisaki and S. Liu, "Magnetic hysteresis curve influenced by power-semiconductor characteristics in pulse-width-modulation inverter," *J. Appl. Phys.*, vol. 115, Feb. 2014, Art. no. 17A321, doi 10.1063/1.4863256.
[6] K. Fujisaki, M. Sakai, and S. Takeda, "Motor loss increment of induction motor driven by PWM inverter in comparison with inverter circuit loss," in *Proc. IEEE 15th Int. Conf. Elect. Mach. Syst.*, Sapporo, Japan, Oct. 2012, pp. 1–6.
[7] A. Boglietti, A. Cavagnino, D. M. Ionel, M. Popescu, D. A. Staton, and S. Vaschetto, "A general model to predict the iron losses in PWM inverter-fed induction motors," *IEEE Trans. Ind. Appl.*, vol. 46, no. 5, pp. 1882–1890, Sep./Oct. 2010, doi 10.1109/TIA.2010.2057393.
[8] E. Dlala and A. Arkkio, "A general model for investigating the effects of the frequency converter on the magnetic iron losses of a squirrel-cage induction motor," *IEEE Trans. Magn.*, vol. 45, no. 9, pp. 3303–3315, Sep. 2009, doi 10.1109/TMAG.2009.2021066.
[9] N. Denis, K. Fujitani, Y. Kato, M. Ieki, and K. Fujisaki, "Core loss increase due to inverter carrier frequency in an interior permanent magnet synchronous motor," in *Proc. IEEE 18th Int. Conf. Elect. Mach. Syst.*, Pattaya, Thailand, Oct. 2015, pp. 1–7, doi 10.1109/ICEMS.2015.7385142.
[10] P. Chen, R. Tang, W. Tong, X. Han, J. Jia, and X. Zhu, "Analysis of losses of permanent magnet synchronous motor with PWM supply," in *Proc. IEEE 17th Int. Conf. Elect. Mach. Syst.*, Hangzhou, China, Oct. 2014, pp. 1119–1124, doi 10.1109/ICEMS.2014.7013638.
[11] D. Sato and J. Itoh, "Total loss comparison of inverter circuit topologies with interior permanent magnet synchronous motor drive system," in *Proc. IEEE ECCE Asia Downunder*, Melbourne, Australia, Jun. 2013, pp. 537–543, doi 10.1109/ECCE-Asia.2013.6579149.
[12] K. Yamazaki and Y. Seto, "Iron loss analysis of interior permanent-magnet synchronous motors—Variation of main loss factors due to driving condition," *IEEE Trans. Ind. Appl.*, vol. 42, no. 4, pp. 1045–1052, Jul./Aug. 2006, doi 10.1109/TIA.2006.876080.
[13] K. Yamazaki, M. Kumagai, T. Ikemi, and S. Ohki, "A novel rotor design of interior permanent-magnet synchronous motors to cope with both maximum torque and iron-loss reduction," *IEEE Trans. Ind. Appl.*, vol. 49, no. 6, pp. 2478–2486, Nov./Dec. 2013, doi 10.1109/TIA.2013.2262662.
[14] S.-J. Lee, S.-I. Kim, and J.-P. Hong, "Investigation on core loss according to stator shape in interior permanent magnet synchronous motor," in *Proc. IEEE Int. Conf. Elect. Mach. Syst.*, Wuhan, China, Oct. 2008, pp. 3158–3161.
[15] S. Chaithongsuk, P. Thounthong, N. Takorabet, and B. Nahid-Mobarakeh, "On the reduction of rotor losses in interior permanent magnet motor design and construction," in *Proc. 18th IEEE Int. Conf. Elect. Mach. Syst.*, Pattaya, Thailand, Oct. 2015, pp. 1–7, doi 10.1109/ICEMS.2015.7385139.
[16] L. Ma, M. Sanada, S. Morimoto, and Y. Takeda, "Prediction of iron loss in rotating machines with rotational loss included," *IEEE Trans. Magn.*, vol. 39, no. 4, pp. 2036–2041, Jul. 2003, doi 10.1109/TMAG.2003.812706
[17] K. Fujisaki, S. Satoh, and M. Enokizono, "Influence of vector magnetic property with rotational magnetic flux, magnetic hysteresis and angle difference on stator core loss," *J. Jpn. Soc. Appl. Electromagn. Mech.*, vol. 20, pp. 360–365, 2012.
[18] T. Tamaki, K. Fujisaki, K. Wajima, and K. Fujiwara, "Comparison of magnetic field analysis methods considering magnetic anisotropy," *IEEE Trans. Magn.*, vol. 46, no. 2, pp. 187–190, Feb. 2010, doi 10.1109/TMAG.2009.2033558.
[19] K. Fujisaki *et al.*, "Motor core iron loss analysis evaluating shrink fitting and stamping by finite-element method," *IEEE Trans. Magn.*, vol. 43, no. 5, pp. 1950–1954, May 2007, doi 10.1109/TMAG.2006.877041.
[20] H. Pfutzner *et al.*, "Automatic 3-D building factor analyses of a grain-oriented model transformer core," *IEEE Trans. Mag.*, vol. 50, no. 4, Apr. 2014, Art. no. 8400604, doi 10.1109/TMAG.2013.2287607.
[21] S. Odawara *et al.*, "Impact of material on the iron losses of a reactor with air gap," *IEEE Trans. Magn.*, vol. 51, no. 11, Nov. 2015, Art. no. 8401404, doi 10.1109/TMAG.2015.2435012.
[22] A. Boglietti, "A first approach for the iron losses building factor determination," in *Conf. Rec. IEEE Ind. Appl. Conf.*, Phoenix, AZ, USA, Oct. 1999, vol. 1, pp. 489–493, doi 10.1109/IAS.1999.799998.
[23] T. Tanaka, S. Koga, R. Kogi, and S. Odawara, "High-carrier-frequency iron-loss characteristics excited by GaN FET single-phase PWM inverter," *IEEJ Trans. Ind. Appl.*, vol. 136, no. 2, pp. 110–117, 2016, doi 10.1541/ieejias.136.110.
[24] K. Yamazaki and A. Abe, "Loss investigation of interior permanent-magnet motors considering carrier harmonics and magnet eddy currents," *IEEE Trans. Ind. Appl.*, vol. 45, no. 2, pp. 659–665, Mar./Apr. 2009, doi 10.1109/TIA.2009.2013550.
[25] E. Barbisio, F. Fiorillo, and C. Ragusa, "Predicting loss in magnetic steels under arbitrary induction waveform and with minor hysteresis loops," *IEEE Trans. Magn.*, vol. 40, no. 4, pp. 1810–1819, Jul. 2004, doi 10.1109/TMAG.2004.830510.
[26] K. Yamazaki and N. Fukushima, "Iron-loss modeling for rotating machines: Comparison between Bertotti's three-term expression and 3-D eddy-current analysis," *IEEE Trans. Magn.*, vol. 46, no. 8, pp. 3121–3124, Aug. 2010, doi 10.1109/TMAG.2010.2044384.
[27] *Magnetic materials - Part 3: Methods of measurement of the magnetic properties of magnetic sheet and strip by means of a single sheet tester,* IEC 60404-3, 2nd ed., 1992.
[28] *Methods of measurement of the magnetic properties of magnetic steel sheet and strip by means of a single sheet tester,* Japanese Industrial Standard C2556, 1996.
[29] S. Odawara, D. Kayamori, and K. Fujisaki, "Influence of sampling frequency on magnetic characteristic evaluation under inverter excitation," *IEEJ Trans. Fundam. Mater.*, vol. 135, no. 7, pp. 385–390, 2015, doi 10.1541/ieejfms.135.385.
[30] M. S. Rylko, B. J. Lyons, J. G. Hayes, and M. G. Egan, "Revised magnetics performance factors and experimental comparison of high-flux materials for high-current DC-DC inductors," *IEEE Trans. Power Electron.*, vol. 26, no. 8, pp. 2112–2126, Aug. 2011, doi 10.1109/TPEL.2010.2103573.

Nicolas Denis (M'12) was born in France in 1987. He received the M.Eng. and French Engineer Diploma degrees in electrical engineering from the École Nationale Supérieure d'Électricité et de Mécanique de Nancy, Nancy, France, in 2010, and the Dr.Eng. degree in electrical engineering from Sherbrooke University, Sherbrooke, QC, Canada, in 2014.

He is currently a Postdoctoral Fellow with Toyota Technological Institute, Nagoya, Japan, working on electrical motors iron losses and applications of efficient magnetic materials for electrical motors.

Shunya Odawara (M'13) was born in 1987. He received the B.Eng., M.Eng., and Dr.Eng. degrees from Saga University, Saga, Japan, in 2009, 2010, and 2013, respectively.

Since 2013, he has been with Toyota Technological Institute, Nagoya, Japan, as a Postdoctoral Researcher. His current research interests include loss characteristics evaluation by inverter excitation taking into account magnetic property and semiconductor property.

Keisuke Fujisaki (S'82–M'83–SM'02) received the B.Eng., M.Eng., and Dr.Eng. degrees in electronics engineering from the Faculty of Engineering, The University of Tokyo, Tokyo, Japan, in 1981, 1983, and 1986, respectively.

From 1986 to 1991, he conducted research on electromagnetic force applications to steelmaking plants at the Ohita Works, Nippon Steel Corporation. From 1991 to 2010, he was a Chief Researcher with the Technical Development Bureau, Nippon Steel Corporation, Futtsu, Japan. Since 2010, he has been a Professor at Toyota Technological Institute, Nagoya, Japan. His current scientific interests include magnetic multiscale, electromagnetic multiphysics, high-efficiency motor drive systems, electrical motors, and power electronics. From 2002 to 2003, he was a Visiting Professor at Ohita University, Oita, Japan. From 2003 to 2009, he was a Visiting Professor at Tohoku University, Sendai, Japan.

Prof. Fujisaki received the Outstanding Prize Paper Award at the Metals Industry Committee sessions of the 2002 IEEE Industry Applications Society Annual Meeting.